The role of integrin-linked kinase in the molecular architecture of focal adhesions

Nadav Elad[1,*], Tova Volberg[2], Israel Patla[1], Vera Hirschfeld-Warneken[3,4], Carsten Grashoff[5], Joachim P. Spatz[3,4], Reinhard Fässler[5], Benjamin Geiger[2,‡] and Ohad Medalia[6,1,‡]

[1]Department of Life Sciences and the National Institute for Biotechnology in the Negev, Ben Gurion University of the Negev, Beer-Sheva 84120, Israel
[2]Department of Molecular Cell Biology, Weizmann Institute of Science, Rehovot 76100, Israel
[3]Department of New Materials and Biosystems, Max-Planck Institute for Intelligent Systems, Stuttgart D-70569, Germany
[4]Department of Biophysical Chemistry, University of Heidelberg, Heidelberg D-70569, Germany
[5]Department of Molecular Medicine, Max-Planck Institute of Biochemistry, Martinsried D-82152, Germany
[6]Department of Biochemistry, University of Zurich, CH-8057 Zurich, Switzerland

*Present address: Center for Human Genetics, KULeuven and Department for Molecular and Developmental Genetics, VIB, Leuven 3000, Belgium
‡Authors for correspondence (benny.geiger@weizmann.ac.il; omedalia@bioc.uzh.ch)

Accepted 12 June 2013
Journal of Cell Science 126, 4099–4107

doi: 10.1242/jcs.120295

Summary

Integrin-mediated focal adhesions (FAs) are large, multi-protein complexes that link the actin cytoskeleton to the extracellular matrix and take part in adhesion-mediated signaling. These adhesions are highly complex and diverse at the molecular level; thus, assigning particular structural or signaling functions to specific components is highly challenging. Here, we combined functional, structural and biophysical approaches to assess the role of a major FA component, namely, integrin-linked kinase (ILK), in adhesion formation. We show here that ILK plays a key role in the formation of focal complexes, early forms of integrin adhesions, and confirm its involvement in the assembly of fibronectin-bound fibrillar adhesions. Examination of ILK-null fibroblasts by cryo-electron tomography pointed to major structural changes in their FAs, manifested as disarray of the associated actin filaments and an increase in the packing density of FA-related particles. Interestingly, adhesion of the mutant cells to the substrate required a higher ligand density than in control cells. These data indicate that ILK has a key role in integrin adhesion assembly and sub-structure, and in the regulation of the FA-associated cytoskeleton.

Key words: Integrin, Cell adhesion, Cryo-electron tomography, Correlated microscopy, Integrin-linked kinase, Focal adhesion

Introduction

Cells adhere to the extracellular matrix (ECM) through integrin-mediated and cytoskeleton-associated structures known as focal adhesions (FAs) (Burridge et al., 1988; Campbell, 2008; Geiger et al., 2009). Beyond their scaffolding function, FAs also serve as sensory structures, which probe the chemical and physical state of the surrounding microenvironment and consequently activate signaling processes that affect multiple cellular features, including survival, proliferation, differentiation and migration (Legate et al., 2009). The structural integrity of FAs, and their scaffolding and sensory functions, depend on large multi-protein complexes linking integrins to F-actin, and regulating both the assembly of the adhesion structures and their signaling activities. Over 180 adhesion-associated proteins have thus far been identified in these adhesion sites (Byron et al., 2011; Schiller et al., 2011; Zaidel-Bar et al., 2007b); yet their precise organization, mode of action, and contributions to the adhesion process are still poorly understood (see: http://www.adhesome.org).

A prominent component of the adhesome is the protein integrin-linked kinase (ILK), a multi-functional molecule that binds directly to the cytoplasmic domains of β1 and β3 integrins, and may associate indirectly with actin through its binding partners, including parvin (Hannigan et al., 1996; Legate et al., 2006; Vakaloglou and Zervas, 2012), paxillin (Nikolopoulos and Turner, 2001) or PINCH (Stanchi et al., 2009). ILK is also reported to play a role in regulating actin and microtubule dynamics and mechanics (Legate et al., 2006; Sayedyahossein et al., 2012; Wickström et al., 2010) by suppressing RhoA-induced actomyosin contractility (Montanez et al., 2009; Aspenström et al., 2004) and stabilizing microtubule tips at nascent FAs (Wickström and Fässler, 2011; Efimov and Kaverina, 2009). Consequently, ILK-deficient fibroblasts have poorly organized actin bundles, associated with attenuated cell spreading. Loss of ILK expression also impairs fibronectin fibrillogenesis (Stanchi et al., 2009; Vouret-Craviari et al., 2004). Knockout of *Ilk* in mice results in lethality at the preimplantation stage, characterized by adhesion and polarity defects of the epiblast, a failure to form the amniotic cavity (Sakai et al., 2003), and involvement in muscle attachment sites (Zervas et al., 2011). However, despite this information, the molecular mechanisms underlying these structural manifestations of ILK depletion have yet to be resolved.

Recently, the fine architecture of FAs in cultured fibroblasts was visualized using super-resolution fluorescence microscopy (Kanchanawong et al., 2010) and cryo-electron tomography (cryo-ET) (Patla et al., 2010). These findings demonstrated that FAs are laminated structures, composed of a dense bundle of actin filaments, well-aligned with their major axis, which is linked to the ventral cell membrane through a layer of large

macro-molecular complexes (termed focal adhesion-related particles; FARPs) (Patla et al., 2010).

The results presented here show that the attenuated spreading of ILK-null cells is associated with a loss of focal complexes and fibrillar adhesions. Furthermore, labeling for multiple adhesome components indicated that *Ilk* knockout leads to a reduction in vinculin levels and an accumulation of the fibrillar adhesions molecule tensin in FA sites. Cryo-ET of *Ilk* knockout cells revealed major disarray of the FA-associated actin filaments, and a 1.7-fold increase in the density of FARPs at the membrane–actin interface. Interestingly, FA formation by ILK-null cells required a similarly higher density of the adhesion-mediating c(-RGDfK) peptide, compared with control cells. These results shed light on the key roles of ILK in regulating FA formation and remodeling, and cytoskeletal organization.

Results

ILK is involved in the formation of integrin-mediated focal complexes

To determine the function of ILK in the development and maturation of integrin-mediated adhesions, we compared the spreading and polarization of cultured mouse kidney fibroblasts carrying a floxed (loxP-flanked) ILK gene ($Ilk^{f/f}$; expressing normal levels of ILK) to their ILK-deficient counterparts (adenoviral Cre deleted; $Ilk^{-/-}$) (Azimifar et al., 2012). When plated on a fibronectin (FN)-coated surface, the $Ilk^{f/f}$ cells underwent progressive spreading (supplementary material Fig. S1A) and then polarized (Fig. 1A,B), just like wild-type mouse fibroblasts. The $Ilk^{-/-}$ cells, however, showed marked delays in spreading and remained generally round (Fig. 1C,D, and supplementary material Fig. S1B). Double-fluorescence labeling for vinculin (Fig. 1; red) and actin (Fig. 1; green) indicated that the ILK-deficient cells initially form aberrant FAs, which are almost exclusively located at the cell periphery, associated with poorly organized F-actin bundles, and clearly distinct from the robust FAs and stress fibers found in the $Ilk^{f/f}$ controls.

In cultured fibroblasts, FA assembly is initiated by the formation of small (typically <1 μm apparent diameter), transient nascent adhesions and focal complexes (FXs) underneath the peripheral lamellipodium (Choi et al., 2008; Geiger et al., 2009; Geiger and Yamada, 2011; Vicente-Manzanares and Horwitz, 2011). A subset of these FXs grows and matures into FAs, which become the primary anchorage sites of contractile stress fibers (Vicente-Manzanares et al., 2009). Careful examination of vinculin immunolabeling in $Ilk^{f/f}$ cells revealed multiple FXs along the leading edges of the cells (Fig. 1A,B), whereas the $Ilk^{-/-}$ cells lacked such peripheral structures (Fig. 1C,D). In these cells, FAs were formed under

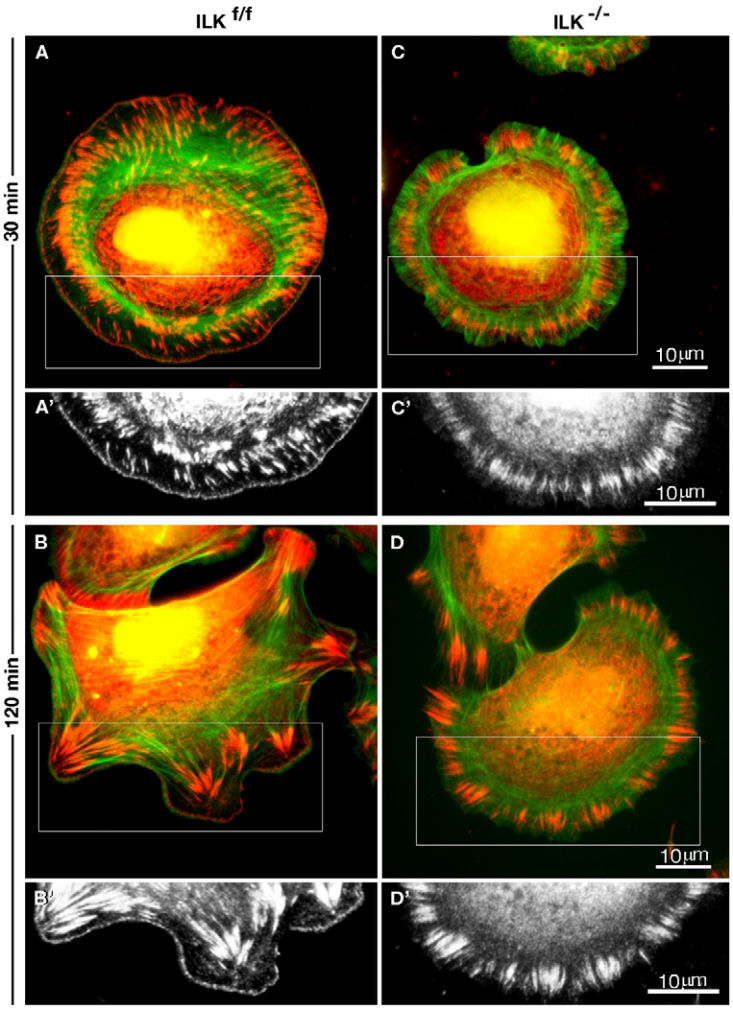

Fig. 1. Deletion of ILK prevents the formation of FXs. $Ilk^{f/f}$ cells (A–B′; $ILK^{f/f}$ in this and subsequent figures) and $Ilk^{-/-}$ cells (C–D′; $ILK^{-/-}$) were cultured on fibronectin-coated coverslips for 30 minutes (A,C) or 120 minutes (B,D), and then permeabilized/fixed and immunolabeled for vinculin (red) and actin (green). Vinculin labeling in the boxed areas in the double-labeled images is shown in A′, B′, C′, D′. Note the multiple FXs along the leading edges of the $Ilk^{f/f}$ cells at early stages of radial spreading (A, 30 minutes), as well as after cell polarization (B, 120 minutes), whereas such peripheral FXs were not formed by the $Ilk^{-/-}$ cells.

retracted lamellae rather than from FXs, as is commonly observed in control cells. This deficiency in FX formation was apparent both during initial radial spreading (Fig. 1C; 30 minutes) and at later stages, when the cells began to polarize (Fig. 1D and supplementary material Fig. S4; Movies 1, 2, for $Ilk^{-/-}$ and $Ilk^{f/f}$, respectively). The lack of FXs in $Ilk^{-/-}$ cells probably accounts for the poor alignment of F-actin within the mutant cells. Indeed, whereas the $Ilk^{f/f}$ control cells developed robust stress fibers (supplementary material Fig. S1A, and Fig. 1A,B), actin bundles in the $Ilk^{-/-}$ cells were less prominent, and poorly organized (supplementary material Fig. S1B; Fig. 1C,D).

ILK is essential for FN fibrillogenesis and for the formation of fibrillar adhesions

A prominent subset of integrin-mediated adhesions formed by cultured fibroblasts (including $Ilk^{f/f}$ cells) with extracellular FN fibrils are known as fibrillar adhesions (FBs) (Vicente-Manzanares et al., 2011; Zaidel-Bar et al., 2004; Zamir et al., 1999). These elongated adhesions extend from the edges of FAs, point toward the cell center, and are enriched with tensin, α5β1 integrin, and dephosphorylated paxillin (Pankov et al., 2000; Zaidel-Bar et al., 2007b). However, the causal interplay between FN fibrillogenesis and the formation of distinct FBs remained unclear.

In line with previous reports (Stanchi et al., 2009; Torgler et al., 2004), we show here that knockout of the ILK gene leads to the apparent inhibition of FN fibrillogenesis, as well as to the loss of tensin-rich FBs (Fig. 2A–H). Furthermore, the absence of ILK (and of FBs) was accompanied by pronounced retention of tensin in FAs, and by a marked reduction in vinculin levels. As shown in Fig. 2I, tensin intensity in FAs was elevated by ~50%, while vinculin intensity decreased by ~50%. Accumulation of tensin in FAs (which are considerably larger than FBs) also resulted in a 60% increase in the apparent area of tensin-rich adhesions in the ILK-null cells, compared with the $Ilk^{f/f}$ controls (Fig. 2J). Interestingly, the expression of vinculin was not effected upon *Ilk* knockout (supplementary material Fig. S3A), whereas the

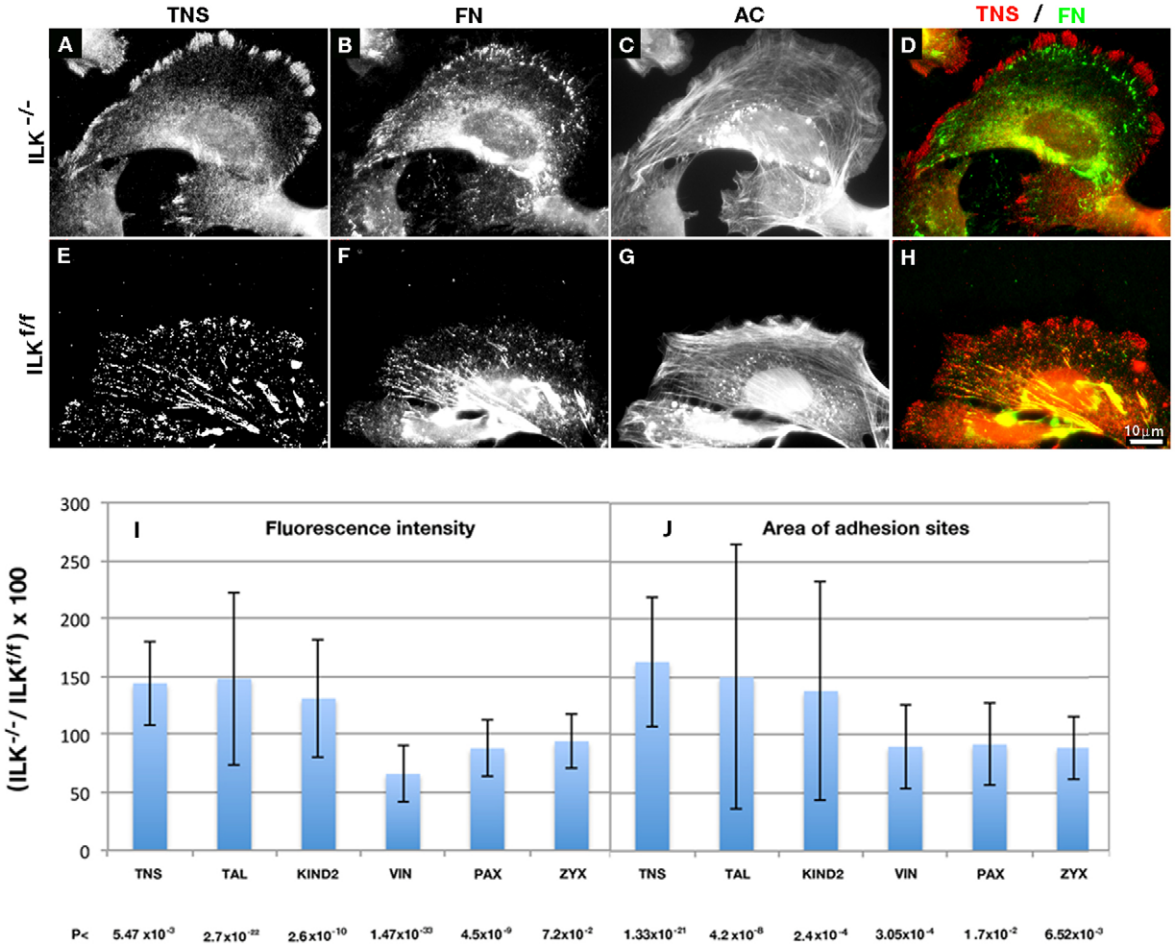

Fig. 2. Effect of *Ilk* knockout on the expression and organization of FA proteins. Upper panel: $Ilk^{-/-}$ (A–D) and $Ilk^{f/f}$ (E–H) cells were cultured on FN-coated coverslips for 16 hours, then permeabilized, fixed and immunolabeled with antibodies against tensin (TNS; A,E), fibronectin (FN; B,F) and with coumarin-tagged phalloidin (AC; C,G). In addition, cells were immunostained with antibodies against tensin, talin, kindlin-2, vinculin, paxillin and zyxin (not shown). Lower panel: histogram showing the intensities (I) and the apparent areas of adhesion sites (H) in $Ilk^{-/-}$ cells, relative to $Ilk^{f/f}$ cells (± standard deviation) of tensin (TNS), talin (TAL), kindlin-2 (KIND2), vinculin (VIN), paxillin (PAX) and zyxin (ZYX). Note the accumulation of labeled tensin in FAs at the cell periphery, and the absence of fibronectin fibrils and FBs. *P*-values are shown at the bottom and point to significant differences in the intensity and area of the different FA proteins in $Ilk^{-/-}$ and $Ilk^{f/f}$ cells. Note the significant increase in tensin concentrations and increased adhesion area (due to its retention in FAs), and the reduced vinculin levels, in the *Ilk* knockout cells.

level of tensin expression increased in the ILK-null cells (supplementary material Fig. S3B)

To further explore the functional hierarchical interplay between ILK, tensin and FN in the formation of FBs, we knocked down FN or tensin in a human fibroblast line, WI-38, and determined the effect of this perturbation on the formation of FBs. As shown in Fig. 3, knockdown of FN led to a complete loss of FN fibrils (despite the fact that FN was present in the culture medium), accompanied by the confinement of both ILK and tensin to bona fide FAs (Fig. 3B,E,H). These cells also failed to form FBs, which were present in control cells (transfected with RNA-induced silencing complex-free siRNA; 'RISC-free'; Fig. 3A,D,G). In contrast, knockdown of tensin did not affect FN fibrillogenesis (Fig. 3C′,F′) or the association of ILK with FBs (Fig. 3C,I). As shown in Fig. 3H′,H, vinculin colocalized with ILK at FAs when FN levels were reduced, but its localization was not affected by tensin knockdown (Fig. 3I′,I). We therefore conclude that ILK-induced assembly of FN fibrils is essential for the formation of FBs, whereas tensin associates with these adhesions, but is not essential for their formation.

Knockout of *Ilk* induces disarray in FA-associated actin filaments

Using cryo-ET (Fridman et al., 2012), we previously demonstrated that FA-associated actin is densely packed into bundles, aligned along the major axis of FAs, and linked by short (~50 nm) interconnecting filaments (Patla et al., 2010). To determine the role of ILK in actin association with FAs, we examined the $Ilk^{-/-}$ fibroblasts by means of cryo-ET, and compared them to both control $Ilk^{f/f}$ fibroblasts, and to untreated cells. Correlative fluorescence microscopy and cryo-ET was used to identify FA locations in $Ilk^{-/-}$ cells expressing YFP–paxillin growing on an FN-coated EM grid. As shown in Fig. 4A, we identified FAs by means of fluorescence microscopy (Fig. 4A,

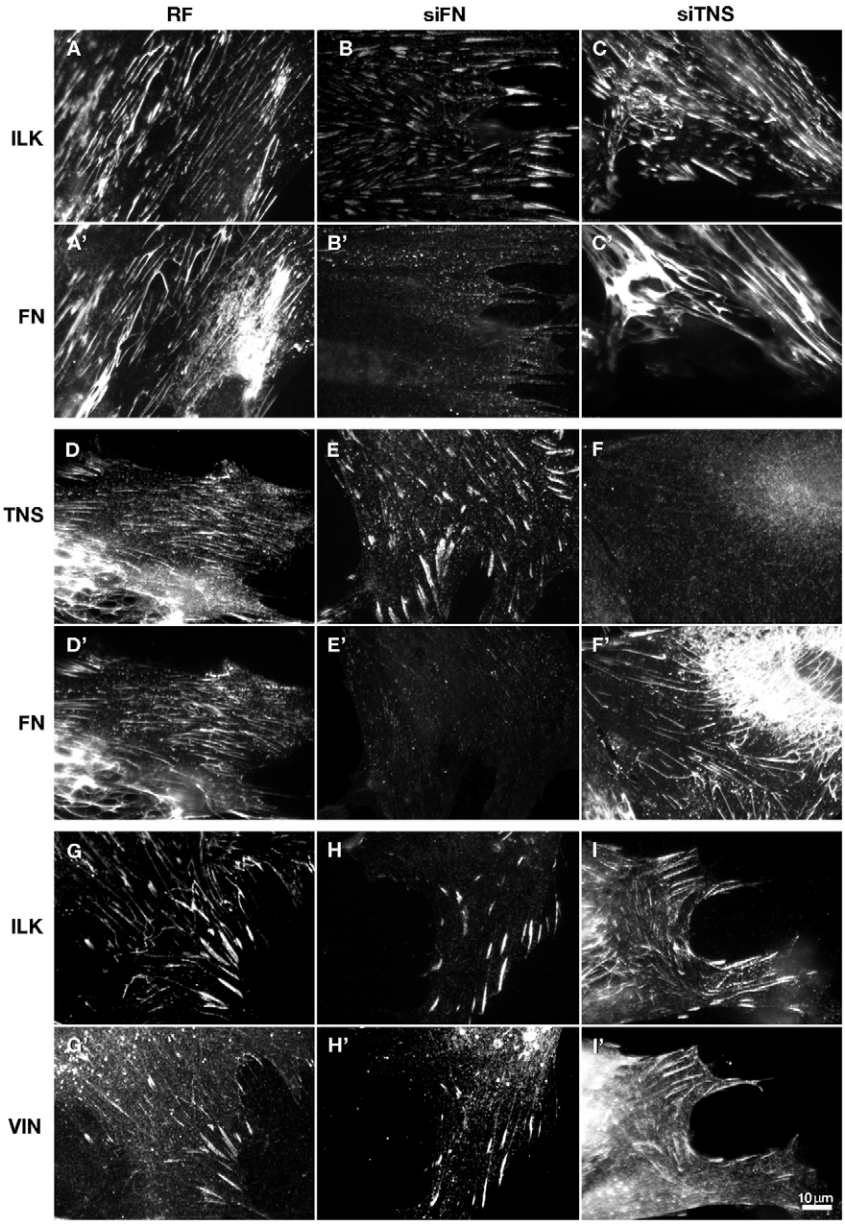

Fig. 3. The differential roles of ILK and tensin in fibronectin fibrillogenesis and FB formation. WI-38 cells were treated with RISC-free (RF) siRNA (A,A′, D,D′, G,G′), siRNA to fibronectin (siFN; B,B′, E,E′, H,H′), or tensin (siTNS; C,C′, F,F′, I,I′), and incubated for 60 hours post-transfection, then trypsinized and replated on FN-coated glass coverslips for an additional 36 hours. Cells were then permeabilized, fixed and double-immunolabeled for ILK and fibronectin (A–C′), tensin and fibronectin (D–F′) and ILK and vinculin (G–I′). Note that knockdown of fibronectin resulted in a complete loss of fibronectin fibrils, as well as ILK- and tensin-rich FBs (B,E). However, knockdown of tensin did not affect fibronectin fibrillogenesis, or the development of ILK-containing FBs (C,C′,F′).

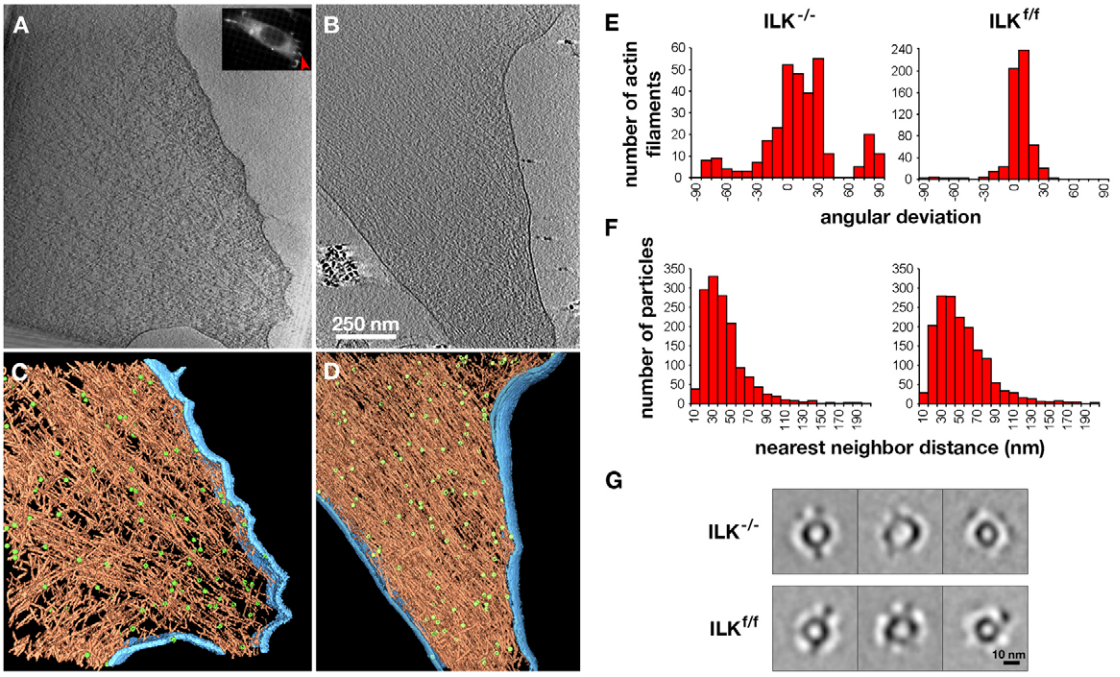

Fig. 4. The molecular architecture of FAs in *Ilk*$^{-/-}$ and *Ilk*$^{f/f}$ fibroblasts. (A,B) 10 nm-thick x-y sections through representative tomograms of central areas of FAs in *Ilk*$^{-/-}$ cells (A) and *Ilk*$^{f/f}$ cells (B). FA sites were identified by correlating electron micrographs with fluorescence microscopy images of YFP–paxillin-expressing cells (A, insert). The red arrowhead in the insert points to the site of the FA tomogram in A. (C,D) Surface rendering view of the FA sites shown in A and B, respectively, as seen from the direction of the substrate toward the cell center. Actin is depicted in tan, membranes in blue, and focal-adhesion-related particles (FARPS) in light green. (E) Histograms representing the orientation of actin filaments within the FA-associated bundle in *Ilk*$^{-/-}$ cells (left) and *Ilk*$^{f/f}$ cells (right). (F) Histograms representing the 'nearest neighbor' distance distribution between individual adhesion-related particles in *Ilk*$^{-/-}$ (left) and *Ilk*$^{f/f}$ cells (right). The average center-to-center distance calculated between particles is 36 nm in *Ilk*$^{-/-}$ and 47 nm in *Ilk*$^{f/f}$ cells. (G) 2D class averages of adhesion-related particles, which were extracted in silico from FA tomograms, and projected along the z-axis. Both the *Ilk*$^{-/-}$ (upper panel) and *Ilk*$^{f/f}$ cells (lower panel) were clearly divided into three main classes with distinct ring diameters (supplementary material Fig. S1A); $n=1037$ and $n=1142$ for *Ilk*$^{-/-}$ and *Ilk*$^{f/f}$ cells, respectively.

inset), froze the samples, inserted them into the cryo-electron microscope, and identified the same FAs at low magnification. An angular set of images was then collected, and subjected to three-dimensional (3D) image reconstruction. One tomographic slice through the reconstructed volume of the FA, positioned a few nanometers above the cell–matrix interface at the cytoplasmic side of the membrane, is shown in Fig. 3A. A surface-rendered view of the same area, in which all observed actin filaments were tracked, is shown in Fig. 4C. A corresponding tomographic slice and a surface-rendered view of an FA from control *Ilk*$^{f/f}$ fibroblasts are shown in Fig. 3B,D, respectively.

The FAs in *Ilk*$^{f/f}$ fibroblasts were normal: and similar to those previously reported for REF52 cells (Patla et al., 2010), with an F-actin bundle, consisting of largely parallel filaments, associated with the central region of the adhesion site. The actin cytoskeleton of *Ilk*$^{-/-}$ fibroblasts, however, was extremely disorganized, and the number of actin filaments per unit area was considerably reduced (by ~70%), compared to wild-type or *Ilk*$^{f/f}$ cells (Fig. 4A,C, compared to B and D). The reduction in the number of filaments was accompanied by a major loss of filament alignment (Fig. 4E) compared with control cells, where the actin filaments were largely aligned along the FA major axis. Quantification of filament alignment indicated a standard deviation of 15° in the *Ilk*$^{f/f}$ cells, compared with ~25° in the *Ilk*$^{-/-}$ cells.

FA-related particles are more densely packed in *Ilk*$^{-/-}$ fibroblasts

FARPs, indistinguishable from those previously reported for REF52 cells (Patla et al., 2010), were observed at the membrane–cytoskeleton interface of both *Ilk*$^{-/-}$ and *Ilk*$^{f/f}$ fibroblasts (Fig. 4C,D, green). Quantification of these particles, however, indicated major differences in their distribution density in control and mutant cells. In control cells, the inter-particle spacing (mean distance between the centers of mass of neighboring particles) was 47±29 nm, similar to the inter-particle spacing measured in REF52 cells (Patla et al., 2010), but in *Ilk*$^{-/-}$ cells the mean inter-particle spacing was 36±17 nm (Fig. 4F).

Notably, despite the apparent 1.3-fold decrease in average FARP spacing in *Ilk*$^{-/-}$ cells, the morphological characteristics of the particles in these mutated cells were highly similar to those found in the WT and *Ilk*$^{f/f}$ cells. We analyzed the structure of the adhesion-related particles in two dimensions by extracting the relevant volumes, and projecting them onto a common plane (Fig. 4G). These images were then aligned, and classified according to principle component analysis. Class averages revealed ring-shaped densities with radiating filaments, which presumably connect the FARPs and the actin bundles (Fig. 4G). In both mutant and control cells, three sources constitute the apparent structural variability between sub-classes of FARPs: the particle diameter, the number of 'whiskers' extending from the particles, and the angular positions of the whiskers. Particles of

both mutated and control cells similarly vary with respect to these three structural features (Fig. 4G and supplementary material Fig. S2). The particles can be classified into three groups of distinct ring diameter, with ratios of 55%, 24% and 21% in $Ilk^{-/-}$ cells, and 30%, 42% and 28% in $Ilk^{f/f}$ cells (Fig. 4G, left to right, respectively; supplementary material Fig. S3A).

The properties of the whiskers in $Ilk^{-/-}$ and $Ilk^{f/f}$ cells were also similar: FARPs of both cell types normally contained 1–5 whiskers per particle, with mean values of 2.89±1.04 and 2.63±0.98 in $Ilk^{-/-}$ and $Ilk^{f/f}$ cells, respectively (supplementary material Fig. S2B). Moreover, the orientations of these whiskers were largely isotropic, although in the $Ilk^{f/f}$ cells, occasional alignment of whiskers along the FA major axis was seen (supplementary material Fig. S2C). Taken together, these data indicate that the altered actin network in $Ilk^{-/-}$ cells is accompanied by higher FARP packing densities; however, the FARPs in both types of cells were indistinguishable, suggesting that ILK is not a crucial component of these structures.

$Ilk^{-/-}$ fibroblasts require a higher density of ECM molecules for effective surface adhesion

To explore the functional significance of the molecular and structural changes induced in FAs by ILK depletion, we tested the adhesion ligand density required for FA formation by $Ilk^{-/-}$ and control cells. It has previously been shown that cells cultured on nano-patterned surfaces, in which the adhesion ligand (cyclic RGD peptide) is positioned at precise inter-spacings (within the range of 20–200 nm), require a particular threshold density to effectively adhere to the surfaces (Arnold et al., 2008; Cavalcanti-Adam et al., 2007). To compare the ligand density requirements of $Ilk^{-/-}$ cells and control $Ilk^{f/f}$ cells, we plated both cell types on nanostructured glass surfaces on which the adhesive peptide ligand [c(-RGDfK); see Materials and Methods] was linked to nanogold particles positioned at fixed inter-spacings. As shown in Fig. 5A,D, $Ilk^{f/f}$ cells plated on surfaces with 32 nm and 52 nm inter-ligand spacings and incubated for 4 hours, spread well on both surfaces (Fig. 5B,E), whereas $Ilk^{-/-}$ cells spread exclusively on surfaces with a 32 nm inter-ligand spacing (Fig. 5C), and failed to adhere and spread on the 52 nm pattern (Fig. 5F). These results indicate that $Ilk^{-/-}$ cells require closer ligand spacing than control cells in order to form functional FAs. Interestingly, these ligand densities are highly similar to the differences in inter-particle spacing found in the mutant and control cells plated on uniform ECMs, and visualized by cryo-ET.

Discussion

ILK is a canonical component of the integrin cell adhesion machinery. Based on this and previous studies, it appears that ILK participates in three distinct stages of integrin adhesion organization: (1) nucleation of FX under the lamellipodium; (2) organization of mature FAs and their associated stress fibers; and (3) induction of FN fibrillogenesis and, consequently, formation of FBs. Specifically, in the absence of ILK, all forms of integrin adhesions will assemble inefficiently, leading not only to slow cell spreading, but also to limited polarization and poor actin alignment.

FN fibrillogenesis is driven by mechanical forces applied to extracellular FN through integrin adhesions (Klotzsch et al., 2009; Ulmer et al., 2008). It was further demonstrated (Zamir et al., 2000) that this process is accompanied by the formation of a special type of integrin adhesion, namely FBs, which extend centripetally from FAs and are transported towards the cell center. The relationship between FBs and FN fibrils has been well established; yet the functional hierarchy between them remained unclear. Here, we show that in the absence of ILK, FN fibrils do not form. As a consequence, tensin, the hallmark of FBs, is confined to and enriched in FAs, although its knockdown has no apparent effect on FN fibrillogenesis, or on the formation of ILK-rich FBs. These results indicate that ILK is an 'upstream regulator', inducing FN fibrillogenesis that, in turn, drives FB formation and the recruitment of molecules such as tensin to these adhesion sites.

The geometry of the ECM has a major effect on the capabilities of cells to adhere.

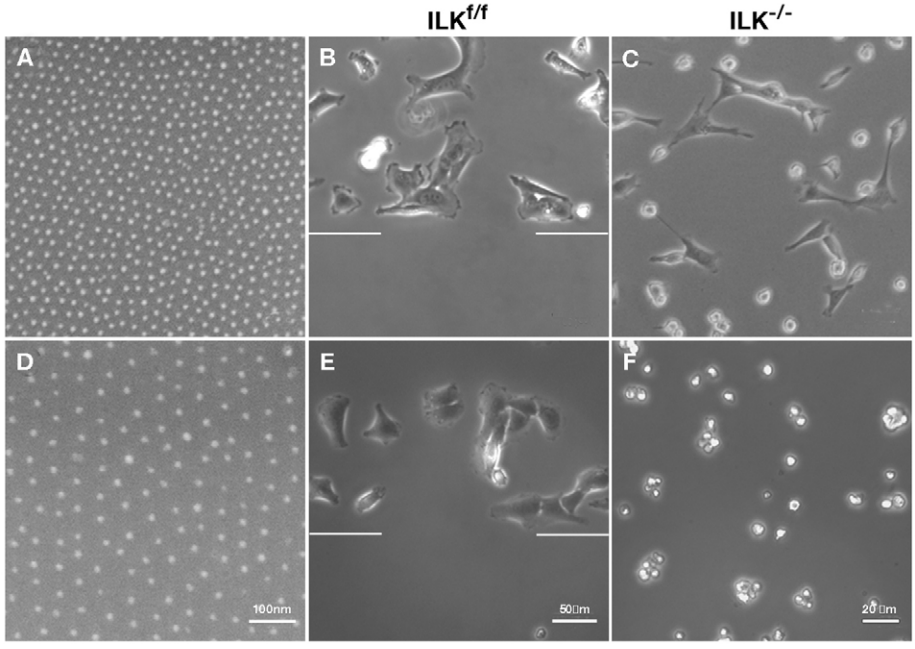

Fig. 5. ILK-deficient cells are highly dependent on the close proximity of surface-bound RGD molecules. (A,D) Scanning electron micrographs showing hexagonally ordered gold nanodots on a glass substrate (dot spacings: 32 and 52 nm, respectively). Similar surfaces were used to study the maximum integrin distances necessary for cell viability. Nano-patterned surfaces were used as a platform for varying RGD inter-ligand patch distances of 32±0.25 nm (A–C), and 52±0.3 nm (D–F). EGFP–paxillin $Ilk^{f/f}$ and EGFP–paxillin $Ilk^{-/-}$ cells were imaged 4 hours after plating on surfaces with 32 nm (B,C) and 52 nm (E,F) inter-ligand spacings, respectively. In B and E, the edges of the functionalized surfaces are marked, to demonstrate the specificity of the assay.

In previous studies on cell adhesion using nano-patterned surfaces it was shown that the formation of genuine FAs is highly sensitive to adhesion ligand density, and occurs when the ligand-to-ligand spacing is on the order of ~50 nm or less (Cavalcanti-Adam et al., 2007). Interestingly, the characteristic spacing between adhesion-related particles within FAs, formed on a uniform matrix is, essentially, the same (Patla et al., 2010). Whether this correlation between the apparent densities of the extracellular molecular tethers to the ECM, and the FARPs interconnecting the membrane and the actin cytoskeleton, has some functional significance, was not clear. Nevertheless, our present findings, showing that in the absence of ILK, both the adhesive ligand [c(-RGDfK)] density needed to induce cell adhesion, spreading and FA formation, and the density of FARPs, increase by ~1.7-fold (from ~450 to 770 FARPs/μm^2), lend further support to the hypothesis that the particles actually bridge between the ECM-bound integrin and the actin network, and that their density is functionally related to the ligand density outside the cell.

The mechanism underlying this ILK-dependent density sensing is still unclear; yet it may be related to the proposed role of ILK in regulating the assembly of adhesome components (Vouret-Craviari et al., 2004; Wang et al., 2008). This is in line with our current results, showing that ILK regulates FARP density, probably without being an essential, intrinsic component of these particles. This conclusion is based on data showing that the FARPs of $Ilk^{-/-}$ and control cells are essentially indistinguishable when examined by cryo-ET. The regulation of FARP density by ILK may be related to a variety of factors, including an overall alteration in FA molecular composition, such as the increase in tensin levels, or the reduction in vinculin levels shown here (possibly due to the arrest of tensin exit during FB formation), as well as to the direct and specific effect of ILK on cytoskeletal organization at the adhesion site.

Taken together, the recent structural mapping of integrin adhesions at nano-scale resolution (Kanchanawong et al., 2010; Patla et al., 2010), the characterization of adhesome complexity and interactivity (Byron et al., 2012; Geiger and Yamada, 2011; Kuo et al., 2011; Schiller et al., 2011; Zaidel-Bar et al., 2007a), and the identification of distinct 'molecular signatures' of subdomains within FAs at micro-scale resolution (Zamir et al., 2008), suggest that integrin adhesions are modular structures, with various molecular complexes displaying distinct distributions and functional roles. Our previous siRNA screen (Winograd-Katz et al., 2009), as well as the findings reported here, demonstrate that specific adhesome components have distinct structural and regulatory roles in the assembly of integrin adhesion structure, and in control of their function. It is conceivable that systematic perturbation of integrin adhesions by gene modulation or different environmental cues, combined with structural analyses such as the one presented here, will become a mainstream approach for characterizing the functional molecular architecture of these sites.

Materials and Methods

Generation of paxillin–EGFP expressing fibroblasts

$Ilk^{f/f}$ and $Ilk^{-/-}$ fibroblasts, stably expressing similar levels of paxillin–EGFP, were prepared by infecting the mutant cells with a retroviral expression vector encoding paxillin–YFP (kindly provided by E. Danen, Leiden University). The VSV-pseudotyped retroviral vectors used for that purpose were produced as previously described (Sakai et al., 2003; Azimifar et al., 2012), and the concentrated viral supernatant, thus produced, was used to infect $Ilk^{f/f}$ fibroblasts. Single clones of $Ilk^{f/f}$ fibroblasts stably expressing paxillin–EGFP were isolated, and subsequently treated with an adenovirus expressing Cre recombinase, in order to delete the ILK gene and to obtain $Ilk^{-/-}$ paxillin–EGFP-expressing fibroblasts.

Cell culture and immunolabeling

Mouse fibroblasts ($Ilk^{f/f}$) expressing EGFP–paxillin, cells deficient in the ILK protein ($Ilk^{-/-}$), and WI-38 cells from human embryonic lung tissue were plated on glass coverslips coated with FN (as indicated). The cells were cultured in Dulbecco's modified Eagle's medium (DMEM; Biological Industries) supplemented with 10% (v/v) fetal calf serum (FCS; Biological Industries), L-glutamine (0.2 M; Biological Industries), and penicillin–streptomycin–nystatin (Biological Industries), at 37℃ and in a 5% CO_2 humidified atmosphere.

Cultured cells were permeabilized, fixed and double-immunolabeled, as previously described (Volberg et al., 2001). Antibodies used included monoclonal antibodies anti-vinculin, rabbit anti-FN and rabbit anti-tensin (produced in the Antibody Production Laboratories, Department of Biological Services, Weizmann Institute of Science), anti-ILK (Santa Cruz Biotechnology, Inc.) and anti-zyxin (kindly provided by Daniel Louvard, Institut Curie, Paris, France). Secondary antibodies used included anti-mouse Cy3 (Jackson ImunoResearch; cat. no. 115-166-072), and anti-rabbit Alexa Fluor 488 (Molecular Probes; cat. no. A11034). To visualize the F-actin cytoskeleton, cells were treated with phalloidin Alexa Fluor 488 (Sigma; cat. no. P1951).

Gene knockdown protocol

WI-38 cells, 3×10^5 cells/well, were cultured in six-well plates coated with 5 µg/ml bovine plasma FN, in DMEM supplemented with 10% FCS (Biological Industries) containing sodium pyruvate, non-essential amino acids, and antibiotics (Sigma) for 24 hours at 37℃.

Cells were transfected with siRNA specific for FN (siFN) or tensin (siTNS; SMARTpools; Dharmacon RNAi Technologies).

Correlative fluorescence and electron microscopy

Carbon-coated 200-mesh gold grids (Quantifoil) were rinsed in PBS (Biological Industries) and overlaid on a drop of 50 µg/ml bovine plasma fibronectin (Biological Industries) for 45 minutes. Cells were typically applied to grids in concentrations of 100 cells per grid, and cultured for 24 hours. Next, specimens were examined by fluorescence microscopy, washed with PBS, and freeze-plunged instantly into liquid-nitrogen-cooled ethane (see below). FAs identified by fluorescence microscopy were indexed according to their precise positions on the grid.

The coordinates of each FA site were recorded and identified under the electron beam. Fluorescence images were acquired with a DeltaVision system (Applied Precision, USA) equipped with a CoolSnap HQ camera (Photometric, USA) operated by SoftWorx and Resolve3D software (Applied Precision), using an Olympus PlanApoN 60×/1.42 NA objective on an Olympus IX70 inverted microscope (Olympus, Japan).

Cryo-electron tomography

A 5 µl drop of BSA-coated 15 nm gold colloids in PBS was added to the grids before plunging them into liquid-nitrogen-cooled ethane, as previously described (Dubochet et al., 1988). Specimens were then transferred into a 300 FEG Polara microscope (FEI, Eindhoven) equipped with a Gatan post-column GIF 2002 energy filter. Tilt series were then collected, typically covering an angular range of −60° to +66°, sampled in 2° tilt increments, and at a 14 µm underfocus. Pixel size was 0.82 nm at the specimen level.

Image processing of cryo-ET images

Projection images (2048×2048 pixels) were aligned to a common origin, using 15 nm-sized fiducial gold particles, and reconstructed by means of weighted back-projection, as implemented by a TOM toolbox software package (Nickell et al., 2005). All tomograms were reconstructed with a binning factor, to yield a 1.64 nm voxel size. For visualization purposes, the reconstructed volumes were processed according to an anisotropic de-noising algorithm (Frangakis and Hegerl, 2001). Individual adhesion complexes were identified and extracted in silico (952 and 946 from mutant and wild-type cells, respectively), from the five best tomograms from each cell line. Two-dimensional images of these elements were calculated by projecting the volumes, 32×32×11 voxels, along the z-axis, using the EM software package. The stack of particles was then masked and normalized prior to PCA, and followed by K-means classification (SPIDER). The most detailed class averages were chosen to be the first references for a multi-reference alignment of the data set. This strategy was iterated for five rounds, until no major changes occurred in the classes, and in the alignment of single images. Surface-rendered visualizations were constructed using AMIRA 5.3 software (Mercury).

Patterned gold surfaces

Gold surfaces were prepared as previously described (Cavalcanti-Adam et al., 2007).

Characterization of nano-structured glass interfaces

Glass samples were sputter-coated with a carbon layer, in preparation for imaging with a field-emission scanning electron microscope (LEO-1530, LEO). To visualize the gold nanoparticles on the surface, an acceleration voltage of 3 kV was applied under a pressure of 5×10^{-6} mbar.

Biofunctionalization

To passivate the substrate area between the gold nanoparticles, polyethylene glycol (PEG; molecular weight 2000) was used (Blümmel et al., 2007). The gold nanoparticles were then functionalized with the cyclic RGD-based peptide c(-RGDfK-), using the spacer aminohexanoic acid, to mercaptopropionic acid. Next, the PEG-functionalized substrates were immersed for 24 hours in a 25-mM c(- RGDfK-)-thiol/water solution. The substrates were then thoroughly rinsed with MilliQ® water for 24 hours.

Cell seeding conditions for nanostructured and biofunctionalized substrates

Cell samples were sterilized in 70% ethanol for 20 minutes, and washed three times with phosphate-buffered saline at room temperature. Cells were then plated at a density of 40 cells/mm^2 in DMEM containing 1% FBS and 1% L-glutamine. Experiments were performed three times. Images were obtained after 4 hours and after 24 hours with an Olympus IX inverted microscope.

Acknowledgements

The authors express gratitude to B. Morgenstern for expert help in preparing this manuscript. B.G. holds the Erwin Neter Professorial Chair in Cell and Tumor Biology. J.S. holds a Weston Visiting Professorship at the Weizmann Institute of Science, Israel.

Author contributions

Experiments were performed by N.E., T.V., I.P., V.H.W. and C.G. The manuscript was written by O.M. and B.G. The study was designed and jointly supervised by J.P.S, R.F., B.G. and O.M.

Funding

This study was supported by the German–Israeli Cooperation Project (DIP H.2.2 to O.M., R.F., J.S. and B.G.); the Israel Science Foundation to B.G.; a European Research Council Starting Grant [grant number 243047 INCEL to O.M.]; the Max Planck Society to R.F. and J.S.; and the European Union Seventh Framework Programme (FP7/2007–2013), [grant number NMP4-LA-2009-229289 NanoII to B.G.].

Supplementary material available online at
http://jcs.biologists.org/lookup/suppl/doi:10.1242/jcs.120295/-/DC1

References

Arnold, M., Hirschfeld-Warneken, V. C., Lohmüller, T., Heil, P., Blümmel, J., Cavalcanti-Adam, E. A., López-García, M., Walther, P., Kessler, H., Geiger, B. et al. (2008). Induction of cell polarization and migration by a gradient of nanoscale variations in adhesive ligand spacing. *Nano Lett.* **8**, 2063-2069.

Aspenström, P., Fransson, A. and Saras, J. (2004). Rho GTPases have diverse effects on the organization of the actin filament system. *Biochem. J.* **377**, 327-337.

Azimifar, S. B., Böttcher, R. T., Zanivan, S., Grashoff, C., Krüger, M., Legate, K. R., Mann, M. and Fässler, R. (2012). Induction of membrane circular dorsal ruffles requires co-signalling of integrin-ILK-complex and EGF receptor. *J. Cell Sci.* **125**, 435-448.

Blümmel, J., Perschmann, N., Aydin, D., Drinjakovic, J., Surrey, T., Lopez-Garcia, M., Kessler, H. and Spatz, J. P. (2007). Protein repellent properties of covalently attached PEG coatings on nanostructured SiO(2)-based interfaces. *Biomaterials* **28**, 4739-4747.

Burridge, K., Fath, K., Kelly, T., Nuckolls, G. and Turner, C. (1988). Focal adhesions: transmembrane junctions between the extracellular matrix and the cytoskeleton. *Annu. Rev. Cell Biol.* **4**, 487-525.

Byron, A., Humphries, J. D., Bass, M. D., Knight, D. and Humphries, M. J. (2011). Proteomic analysis of integrin adhesion complexes. *Sci. Signal.* **4**, pt2.

Byron, A., Humphries, J. D., Craig, S. E., Knight, D. and Humphries, M. J. (2012). Proteomic analysis of α4β1 integrin adhesion complexes reveals α-subunit-dependent protein recruitment. *Proteomics* **12**, 2107-2114.

Campbell, I. D. (2008). Studies of focal adhesion assembly. *Biochem. Soc. Trans.* **36**, 263-266.

Cavalcanti-Adam, E. A., Volberg, T., Micoulet, A., Kessler, H., Geiger, B. and Spatz, J. P. (2007). Cell spreading and focal adhesion dynamics are regulated by spacing of integrin ligands. *Biophys. J.* **92**, 2964-2974.

Choi, C. K., Vicente-Manzanares, M., Zareno, J., Whitmore, L. A., Mogilner, A. and Horwitz, A. R. (2008). Actin and alpha-actinin orchestrate the assembly and maturation of nascent adhesions in a myosin II motor-independent manner. *Nat. Cell Biol.* **10**, 1039-1050.

Dubochet, J., Adrian, M., Chang, J. J., Homo, J. C., Lepault, J., McDowall, A. W. and Schultz, P. (1988). Cryo-electron microscopy of vitrified specimens. *Q. Rev. Biophys.* **21**, 129-228.

Efimov, A. and Kaverina, I. (2009). Significance of microtubule catastrophes at focal adhesion sites. *Cell Adh. Migr.* **3**, 285-287.

Frangakis, A. S. and Hegerl, R. (2001). Noise reduction in electron tomographic reconstructions using nonlinear anisotropic diffusion. *J. Struct. Biol.* **135**, 239-250.

Fridman, K., Mader, A., Zwerger, M., Elia, N. and Medalia, O. (2012). Advances in tomography: probing the molecular architecture of cells. *Nat. Rev. Mol. Cell Biol.* **13**, 736-742.

Geiger, B. and Yamada, K. M. (2011). Molecular architecture and function of matrix adhesions. *Cold Spring Harb. Perspect. Biol.* **3**, a005033.

Geiger, B., Spatz, J. P. and Bershadsky, A. D. (2009). Environmental sensing through focal adhesions. *Nat. Rev. Mol. Cell Biol.* **10**, 21-33.

Hannigan, G. E., Leung-Hagesteijn, C., Fitz-Gibbon, L., Coppolino, M. G., Radeva, G., Filmus, J., Bell, J. C. and Dedhar, S. (1996). Regulation of cell adhesion and anchorage-dependent growth by a new beta 1-integrin-linked protein kinase. *Nature* **379**, 91-96.

Kanchanawong, P., Shtengel, G., Pasapera, A. M., Ramko, E. B., Davidson, M. W., Hess, H. F. and Waterman, C. M. (2010). Nanoscale architecture of integrin-based cell adhesions. *Nature* **468**, 580-584.

Klotzsch, E., Smith, M. L., Kubow, K. E., Muntwyler, S., Little, W. C., Beyeler, F., Gourdon, D., Nelson, B. J. and Vogel, V. (2009). Fibronectin forms the most extensible biological fibers displaying switchable force-exposed cryptic binding sites. *Proc. Natl. Acad. Sci. USA* **106**, 18267-18272.

Kuo, J. C., Han, X., Hsiao, C. T., Yates, J. R., III and Waterman, C. M. (2011). Analysis of the myosin-II-responsive focal adhesion proteome reveals a role for β-Pix in negative regulation of focal adhesion maturation. *Nat. Cell Biol.* **13**, 383-393.

Legate, K. R., Montañez, E., Kudlacek, O. and Fässler, R. (2006). ILK, PINCH and parvin: the tIPP of integrin signalling. *Nat. Rev. Mol. Cell Biol.* **7**, 20-31.

Legate, K. R., Wickström, S. A. and Fässler, R. (2009). Genetic and cell biological analysis of integrin outside-in signaling. *Genes Dev.* **23**, 397-418.

Montanez, E., Wickström, S. A., Altstätter, J., Chu, H. and Fässler, R. (2009). Alpha-parvin controls vascular mural cell recruitment to vessel wall by regulating RhoA/ROCK signalling. *EMBO J.* **28**, 3132-3144.

Nickell, S., Förster, F., Linaroudis, A., Net, W. D., Beck, F., Hegerl, R., Baumeister, W. and Plitzko, J. M. (2005). TOM software toolbox: acquisition and analysis for electron tomography. *J. Struct. Biol.* **149**, 227-234.

Nikolopoulos, S. N. and Turner, C. E. (2001). Integrin-linked kinase (ILK) binding to paxillin LD1 motif regulates ILK localization to focal adhesions. *J. Biol. Chem.* **276**, 23499-23505.

Pankov, R., Cukierman, E., Katz, B. Z., Matsumoto, K., Lin, D. C., Lin, S., Hahn, C. and Yamada, K. M. (2000). Integrin dynamics and matrix assembly: tensin-dependent translocation of alpha(5)beta(1) integrins promotes early fibronectin fibrillogenesis. *J. Cell Biol.* **148**, 1075-1090.

Patla, I., Volberg, T., Elad, N., Hirschfeld-Warneken, V., Grashoff, C., Fässler, R., Spatz, J. P., Geiger, B. and Medalia, O. (2010). Dissecting the molecular architecture of integrin adhesion sites by cryo-electron tomography. *Nat. Cell Biol.* **12**, 909-915.

Sakai, T., Li, S., Docheva, D., Grashoff, C., Sakai, K., Kostka, G., Braun, A., Pfeifer, A., Yurchenco, P. D. and Fässler, R. (2003). Integrin-linked kinase (ILK) is required for polarizing the epiblast, cell adhesion, and controlling actin accumulation. *Genes Dev.* **17**, 926-940.

Sayedyahossein, S., Nini, L., Irvine, T. S. and Dagnino, L. (2012). Essential role of integrin-linked kinase in regulation of phagocytosis in keratinocytes. *FASEB J.* **26**, 4218-4229.

Schiller, H. B., Friedel, C. C., Boulegue, C. and Fässler, R. (2011). Quantitative proteomics of the integrin adhesome show a myosin II-dependent recruitment of LIM domain proteins. *EMBO Rep.* **12**, 259-266.

Stanchi, F., Grashoff, C., Nguemeni Yonga, C. F., Grall, D., Fässler, R. and Van Obberghen-Schilling, E. (2009). Molecular dissection of the ILK-PINCH-parvin triad reveals a fundamental role for the ILK kinase domain in the late stages of focal-adhesion maturation. *J. Cell Sci.* **122**, 1800-1811.

Torgler, C. N., Narasimha, M., Knox, A. L., Zervas, C. G., Vernon, M. C. and Brown, N. H. (2004). Tensin stabilizes integrin adhesive contacts in Drosophila. *Dev. Cell* **6**, 357-369.

Ulmer, J., Spatz, J. P. and Geiger, B. (2008). Force-induced fibronectin fibrillogenesis in vivo. *Soft Matter* **4**, 1998-2007.

Vakaloglou, K. and Zervas, C. (2012). Parvin-ILK: An intimate relationship. *BioArchitecture* **2**, 91-94.

Vicente-Manzanares, M. and Horwitz, A. R. (2011). Adhesion dynamics at a glance. *J. Cell Sci.* **124**, 3923-3927.

Vicente-Manzanares, M., Choi, C. K. and Horwitz, A. R. (2009). Integrins in cell migration – the actin connection. *J. Cell Sci.* **122**, 199-206.

Vicente-Manzanares, M., Newell-Litwa, K., Bachir, A. I., Whitmore, L. A. and Horwitz, A. R. (2011). Myosin IIA/IIB restrict adhesive and protrusive signaling to generate front-back polarity in migrating cells. *J. Cell Biol.* **193**, 381-396.

Volberg, T., Romer, L., Zamir, E. and Geiger, B. (2001). pp60(c-src) and related tyrosine kinases: a role in the assembly and reorganization of matrix adhesions. *J. Cell Sci.* **114**, 2279-2289.

Vouret-Craviari, V., Boulter, E., Grall, D., Matthews, C. and Van Obberghen-Schilling, E. (2004). ILK is required for the assembly of matrix-forming adhesions and capillary morphogenesis in endothelial cells. *J. Cell Sci.* **117**, 4559-4569.

Wang, H. V., Chang, L. W., Brixius, K., Wickström, S. A., Montanez, E., Thievessen, I., Schwander, M., Müller, U., Bloch, W., Mayer, U. et al. (2008).

Integrin-linked kinase stabilizes myotendinous junctions and protects muscle from stress-induced damage. *J. Cell Biol.* **180**, 1037-1049.

Wickström, S. A. and Fässler, R. (2011). Regulation of membrane traffic by integrin signaling. *Trends Cell Biol.* **21**, 266-273.

Wickström, S. A., Lange, A., Hess, M. W., Polleux, J., Spatz, J. P., Krüger, M., Pfaller, K., Lambacher, A., Bloch, W., Mann, M. et al. (2010). Integrin-linked kinase controls microtubule dynamics required for plasma membrane targeting of caveolae. *Dev. Cell* **19**, 574-588.

Winograd-Katz, S. E., Itzkovitz, S., Kam, Z. and Geiger, B. (2009). Multiparametric analysis of focal adhesion formation by RNAi-mediated gene knockdown. *J. Cell Biol.* **186**, 423-436.

Zaidel-Bar, R., Cohen, M., Addadi, L. and Geiger, B. (2004). Hierarchical assembly of cell-matrix adhesion complexes. *Biochem. Soc. Trans.* **32**, 416-420.

Zaidel-Bar, R., Itzkovitz, S., Ma'ayan, A., Iyengar, R. and Geiger, B. (2007a). Functional atlas of the integrin adhesome. *Nat. Cell Biol.* **9**, 858-867.

Zaidel-Bar, R., Milo, R., Kam, Z. and Geiger, B. (2007b). A paxillin tyrosine phosphorylation switch regulates the assembly and form of cell-matrix adhesions. *J. Cell Sci.* **120**, 137-148.

Zamir, E., Katz, B. Z., Aota, S., Yamada, K. M., Geiger, B. and Kam, Z. (1999). Molecular diversity of cell-matrix adhesions. *J. Cell Sci.* **112**, 1655-1669.

Zamir, E., Katz, M., Posen, Y., Erez, N., Yamada, K. M., Katz, B. Z., Lin, S., Lin, D. C., Bershadsky, A., Kam, Z. et al. (2000). Dynamics and segregation of cell-matrix adhesions in cultured fibroblasts. *Nat. Cell Biol.* **2**, 191-196.

Zervas, C. G., Psarra, E., Williams, V., Solomon, E., Vakaloglou, K. M. and Brown, N. H. (2011). A central multifunctional role of integrin-linked kinase at muscle attachment sites. *J. Cell Sci.* **124**, 1316-1327.